Facies (2019) 65:1
https://doi.org/10.1007/s10347-018-0543-2

ORIGINAL ARTICLE

Stratigraphic evolution of a Brazilian carbonate platform during the Cretaceous: the late Albian–early Turonian of the Sergipe–Alagoas Basin

Bruno Valle[1] · Patrick Führ Dal' Bó[1] · Marcelo Mendes[1] · Julia Favoreto[1] · Ariely Luparelli Rigueti[1] · Leonardo Borghi[1] · Roberto Silva Jr.[2]

Received: 21 May 2018 / Accepted: 17 October 2018 / Published online: 1 November 2018

Abstract
The Cretaceous of Brazil is widely known for vast carbonate platforms that developed along the Brazilian east coast. An onshore well drilled and logged in Sergipe State on a structural low allowed the recovery and study of a continuous 439-m core section that records an interval aged from the late Albian to the early Turonian. The section is characterized by calcilutites, marls, and shales, with occasional carbonate breccias. Ten sedimentary microfacies were recognized that indicate deposition in a deep-marine paleoenvironment constantly affected by gravitational flows. These deposits were influenced by climatic variation, as suggested by the alternation of micritic and clayey layers. The analysis of the vertical microfacies pattern, supported by well logs and geochemistry analyses, led to the subdivision of the core into three third-order depositional sequences. A long-term sea-level rise trend in the studied interval, which records the evolution of a partially protected carbonate-siliciclastic mixed platform to a distally steepened carbonate ramp, is proposed herein. The conclusion obtained by this study is important to the understanding of carbonate platform evolution, with the integrated approach of microfacies, geochemistry, and well logs proving to be essential in obtaining precise information when working with deep-marine deposits.

Keywords Carbonate platform · Sedimentary microfacies · Paleoenvironmental evolution · Cretaceous of Brazil · Sergipe–Alagoas Basin · Cotinguiba Formation · Riachuelo Formation

Introduction

Many carbonate platforms have developed around the world throughout geological history. Numerous authors have studied carbonate platform deposits and proposed useful models to classify and explain their evolution (see Ahr 1973; Wilson 1975; Read 1982; Tucker 1985; Carozzi 1989). Despite the proposed models and their associated facies being widely used, the application of such models to a particular case study should be performed with caution since there are variables (i.e., tectonics, eustatic sea-level changes, climate, sedimentation rate) not accounted for in these models that can severely affect the way that platforms develop and evolve in each particular case.

During the formation of the South Atlantic Ocean, many sedimentary basins developed at the continental margin of Brazil, with an establishment of vast carbonate platforms in most of these basins during the Cretaceous due to the development of suitable conditions for carbonate deposition (i.e., a warm and dry climate). The Sergipe–Alagoas Basin is the one with the more complete Cretaceous carbonate sections exposed onshore, represented by the Riachuelo and Cotinguiba formations; thus, the comprehension of its evolution is essential for a better understanding of the eastern continental margin of Brazil and Cretaceous carbonate platforms in general.

The Albian–Turonian interval is globally known for showing records of important events that occurred during the Cretaceous and changed the sedimentation pattern in carbonate platforms. Intervals of black shales with high total organic carbon (TOC) are described and correlated

✉ Bruno Valle
bruno@geologia.ufrj.br

[1] Laboratory of Sedimentary Geology (Lagesed), Department of Geology, Institute of Geoscience, Federal University of Rio de Janeiro, Rio de Janeiro 21941-916, Brazil

[2] Labmicro, Department of Geology, Institute of Geoscience, Federal University of Rio de Janeiro, Rio de Janeiro 21941-916, Brazil

in many sections around the world, corroborating a global implication for these events (e.g., Ocean Anoxic Event 2 and the maximum global sea level; Schlanger and Jenkyns 1976; Haq 2014). The study of this section is of great importance in understanding the paleoenvironmental changes and evolution of a sedimentary basin through time.

This study was the first developed in Brazil that used a 439-m-thick continuous well core section to present geochemical, well log, and sedimentological data to support the evolution of a carbonate platform, from the late Albian to the early Turonian, exhibiting the expressions of a sea-level rise and a possible oceanic anoxic event correlated globally (Koutsoukos et al. 1991). The presented data are related to a section of the Riachuelo and Cotinguiba Formations and provides information that helps understand the evolution of the Sergipe–Alagoas Basin during the Cretaceous and the effects of particular events acting on a carbonate platform through time.

Geological setting

The Sergipe–Alagoas Basin is located in the northeast Brazilian margin and lies between latitudes 9°S and 12°S and longitudes 35°E and 38°E. It measures ca. 53,000 km^2, of which 40,000 km^2 is located offshore and 13,000 km^2 onshore (Fig. 1).

The geologic evolution of the Sergipe–Alagoas Basin is related to the opening of the South Atlantic Ocean and is part of an extensional basin system that operated during the end of the Jurassic and through the Early Cretaceous (Lana 1990). The basin is formed by a network of half-grabens with a regional dip towards the southeast (Ojeda and Fugita 1976) and a predominance of synthetic faults over antithetic faults, forming a series of structural highs and lows (e.g., the Divina Pastora Low, Fig. 1). Its structural framework comprises a north–south fault system intersected by east–west and northeast–southwest faults (Lana 1990).

The Divina Pastora is a structural low located in the southwest portion of the Sergipe–Alagoas Basin and is

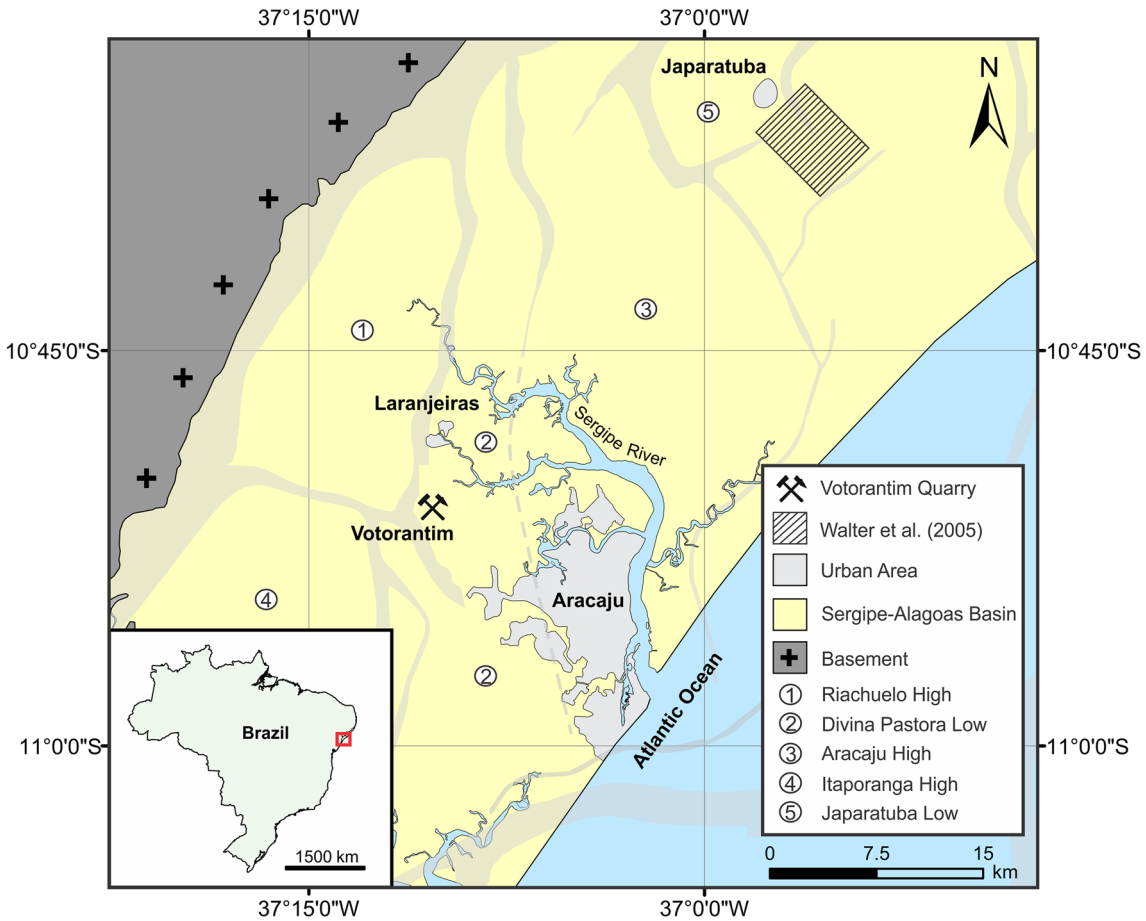

Fig. 1 Location map of the Votorantim quarry with the structural elements of the Sergipe–Alagoas Basin (northeast Brazil), displaying its fault zones in *light gray* and the structural highs and lows in *numbers*

bounded to the west by the Itaporanga and Riachuelo Highs and to the east by the Aracaju and Santa Rosa de Lima Highs, establishing an elongated north–south trend concordant to the main fault system (Lana 1990). It displays a complete stratigraphic section and is an important study location for understanding the Sergipe–Alagoas Basin evolution.

In relation to the other Brazilian continental east margin basins, the Sergipe–Alagoas contains one of the more complete stratigraphic records and has its tectono-stratigraphic evolution divided by Campos Neto et al. (2008) into five sequences: Paleozoic, Pre-Rift, Rift, Post-Rift, and Drift. The studied units, the Riachuelo and Cotinguiba Formations, are part of the Drift sequence; thus, this paper focuses on the Drift phase of the Sergipe–Alagoas Basin.

The Drift phase began during the late Albian and resulted in the effective rupture of continental crust between Brazil and Africa. By that time, warm and dry climatic conditions led to the formation of extensive high-energy carbonate platforms represented by calcarenites, marls, shales, sandstones, and conglomerates attributed to the Riachuelo Formation. This formation is interpreted as a carbonate-siliciclastic mixed platform exhibiting high lateral facies variation and is divided into three members: Angico, Maruim, and Taquari (Campos Neto et al. 2008). The Angico Member is formed by sandstones and conglomerates deposited in fan deltas at the basin edge. The Maruim Member is formed by oolitic and oncolitic calcarenites with isolated algal patches and locally dolomitized by diagenetic events. This member was deposited in high-energy oolitic shoals on structural highs. The Taquari Member is composed of marls and shales representing the deposits of the deeper portions of the basin such as protected lagoons or slopes (Koutsoukos et al. 1993; Campos Neto et al. 2008).

A global sea-level highstand event occurred during the early Cenomanian with a peak in Turonian and drowned the shallow water Riachuelo platform, depositing fine-grained sediments on the carbonate ramp of the Cotinguiba Formation (Koutsoukos 1989). The Cotinguiba Formation is mainly composed of calcilutites, marls, and shales, with intervals rich in foraminiferans, calcispheres, and radiolarians. It is divided into two members: Sapucari and Aracaju (Schaller 1970). The Sapucari Member is composed of gray to bluish gray carbonates with local thickness up to 1,000 m. It consists of massive to laminated carbonates locally interbedded with horizons of cherts, coquinas, and intraformational breccias (Berthou and Bengtson 1988; Walter 2000; Walter et al. 2005). The Aracaju Member is composed of laminated carbonates, marls, and organic-rich shales (Bandeira 1978). The distribution of the rocks constituting this member is restricted to structural lows (e.g., the Divina Pastora Low) and in offshore portions of this basin, representing a more distal facies (Koutsoukos et al. 1993). The sediments of the Cotinguiba Formation were deposited during the Cenomanian–Coniacian in the neritic to upper bathyal portions of a carbonate ramp with hypoxic to anoxic bottom conditions and well-oxygenated epipelagic waters (Koutsoukos et al. 1991).

Materials and methods

This study presents sedimentological, well log (gamma ray), geochemistry, and microfacies analyses of a continuous 439-m-thick well core drilled in the Votorantim quarry (Fig. 1), which outcrops have been studied by many authors in past years (cf. Bengtson 1983; Hessel 1988; Berthou and Bengtson 1988; Andrade 2005). The core 2-LRJ-1-SE is 63 mm in diameter and is stored in the Laboratory of Sedimentary Geology (Lagesed) at the Federal University of Rio de Janeiro (Brazil).

The core description was performed at 1:40 scale to describe high-frequency sedimentological changes. The macro- and mesoscale features described include: lithology, texture, sediment color (Munsell system), sedimentary structures, fossiliferous content, bed thickness, and boundaries. The lithological classification was in accordance with Grabau (1904).

The main described lithotypes were sampled, and 132 thin-sections (see Fig. 2; sampled intervals) were prepared (impregnated with blue-epoxy) at Solintec© laboratories. The petrographic analysis involved the following: (1) recognition of primary and diagenetic constituents, sedimentary structures, textures (Embry and Klovan 1972), clay content and calcite-dolomite proportion according to Friedman's (1959) technique (staining with Alizarin Red-S) and (2) microfacies characterization (Flügel 2004). The quantification method was purely qualitative, and the allochem abundance followed the ACFOR scale (abundant for > 30%; common for 25–35%; frequent for 15–25%; occasional for 5–15%; and rare for < 5%).

For biostratigraphy, 78 samples were systematically collected every 6 m and processed for nannofossil analysis, following the methodology of Alves et al. (2016). In this study, the biostratigraphic framework followed the standard zonations of Burnett (1998) and Antunes (1997).

For geochemical analyses, 147 bulk rock samples were systematically collected every 3 m (Fig. 2). They were crushed and macerated using an agate mill and dried at 80 °C for 4 h. The analyses were conducted at the Chemostratigraphy and Organic Chemistry Laboratory (LGQM) at State University of Rio de Janeiro (UERJ). The samples were dissolved in hydrochloric acid (50% of HCl) to eliminate the calcite and dolomite content and measure the carbonate volume and the insoluble residue (IR), which is basically organic matter, sulfur, quartz, and clay minerals. The total organic carbon (TOC) and total

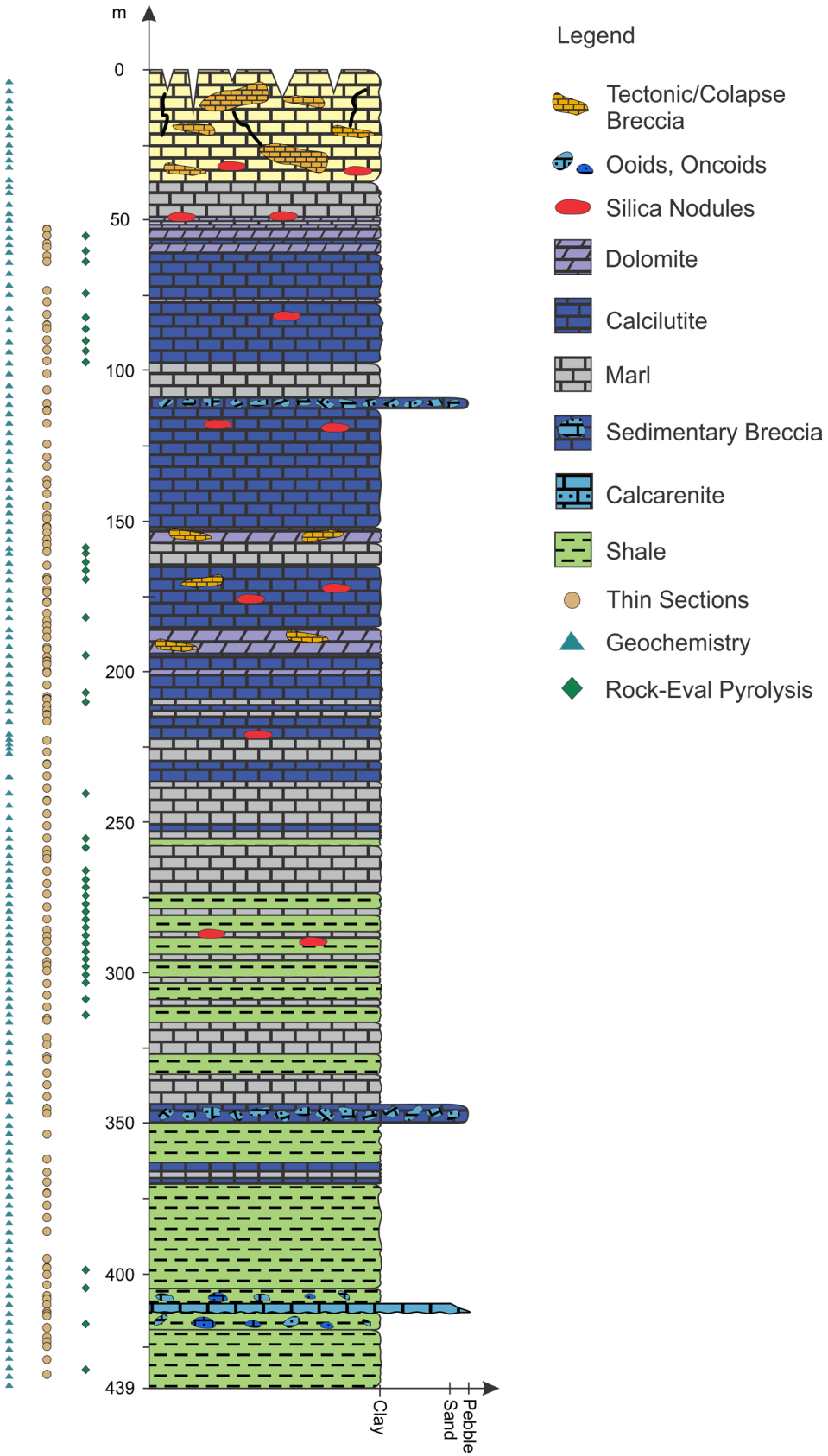

Fig. 2 Schematic sedimentary log showing the lithology distribution and the locations of samples for laboratory analyses

sulfur (S) were then measured in the previously acidized samples with a LECO SC-632 analyzer. Rock–Eval pyrolysis was conducted in every sample (42 in total) with a TOC higher than 1%. This method focused on the quantification of free hydrocarbons in the rock, the quantification of hydrocarbons produced by thermal cracking of the organic matter and the amount of oxygen present in the kerogen. Rock–Eval 6 standard equipment was used and the results were certified with the IFP 160000 standard.

The geophysical gamma ray (wireline) well log was used to calculate the shale volume (linear model), which is an important tool to understand argilosity changes at the studied section. The linear model uses a rule of three to calculate the shale volume (Vsh): a 100% shale volume is attributed to the maximum gamma ray measurement, a 0% shale volume is attributed to the minimum value, and any log measurement between the maximum and minimum is considered to have a shale volume with a proportional variation from 0 to 100% (Poupon and Gaymard 1970). The estimated shale volume was further calibrated based on the carbonate content and insoluble residue results obtained from the geochemistry analysis.

The sequence stratigraphic framework was constructed based on the concepts of Galloway (1989), which consider a genetic stratigraphic sequence as a unit bounded by two stratigraphic surfaces of maximum marine flooding. The use of the genetic stratigraphy sequences of Galloway (1989) was chosen because features indicative of subaerial exposure or linked to regressive surfaces are absent in the studied section. The analysis of microfacies, supported by the gamma ray and geochemistry analyses, allowed the recognition of three third-order sequences, which provided a better understanding of the paleoenvironmental changes and stratigraphic evolution at the Divina Pastora Low from late Albian to early Turonian.

Results

Microfacies characterization

Based on macroscopic and petrographic description, ten microfacies (MF) were identified in the studied section: six of carbonate composition, two of terrigenous composition, and two of hybrid composition. The microfacies are summarized in Table 1. The microfacies organization was based on composition, fossiliferous content, and energy of deposition, with the objective of identifying large-scale environmental changes.

Description

The microfacies *MF 1* (*Crystalline dolomite*) is composed mainly of dolomite with the original rock texture mostly obliterated (Fig. 4a), sometimes showing a primary parallel lamination (Fig. 3a). The dolomite crystals are mostly euhedral and zoned; however, subhedral and anhedral crystals may occur. Bioclasts are rarely described. This microfacies is highly faulted and fractured, exhibiting mostly partially or completely cemented fractures. Berthou and Bengtson (1988) and Walter (2000) noted dolomitized intervals; however, these previous works did not individualize it as a microfacies.

The floatstone lithotypes are represented by two different microfacies, both matrix-supported with massive structure and differentiated mostly by the main components, bioclasts or intraclasts. The microfacies MF 2 (bioclastic floatstone) is characterized by frequent bioclasts, mainly similar-sized macrofossil remains (mostly bivalves) with a chaotic orientation, more than 2 mm in diameter (Fig. 4b) and sometimes fragmented. It is compared to microfacies L Tur A of Berthou and Bengtson (1988) and microfacies type 3 of Walter (2000). The microfacies MF 3 (intraclastic floatstone) consists of gravel-sized intraclasts of peloidal grainstones, peloidal packstones, and wackestones (Fig. 3b). It is poorly sorted with the presence of very fine to very coarse sand-sized peloids, ooids and oncoids. Berthou and Bengtson (1988) described brecciated or coarsely intraclastic limestones in many localities; however, they did not establish microfacies of this nature.

The microfacies MF 4 (graded grain- to packstone) is composed of poorly sorted grainstones and packstones with a basal erosive contact and crude normal grading (from granule to fine-grained sand) (Fig. 3c). Ooids, oncoids, and intraclasts are the predominant allochems (Fig. 4d); however, peloids and bioclasts also occur. Mud intraclasts (20–40 mm in diameter) are concentrated at the base. Dolomitization had occurred, replacing the original blocky calcite cement. This microfacies type was recognized by neither Berthou and Bengtson (1988) nor Walter (2000).

Mudstones and wackestones are represented by microfacies MF 5 (mudstone/wackestone) and MF 6 (argillaceous mudstone/wackestone) and are distinguished mostly by the terrigenous clay content. The fossiliferous content is similar in both microfacies and the matrix is often neomorphized or slightly dolomitized. These microfacies present fractures in a few intervals that are mostly cemented. The microfacies MF 5 is typically burrowed and can exhibit massive or laminated sedimentary structure (Figs. 4e, f). It is compared to microfacies Cen B, Cen D, Cen E, and Cen F of Berthou and Bengtson (1988) and microfacies type 2 of Walter (2000). On the other hand, MF 6 is always laminated and

Table 1 Summary of the described microfacies

Microfacies	Bioclasts	Clay content (%)	Quartz content (silt-sized) (%)	Early diagenetic pyrite
MF 1: Crystalline dolomite	Rare calcified radiolarians, planktonic foraminifera, calcispheres, inoceramids, and echinoids	0–15	–	Rare to abundant
MF 2: Bioclastic floatstone	Abundant bivalve shells. Frequent fish remains. Rare calcispheres, ostracods, and echinoids	0	< 1	Rare
MF 3: Intraclastic floatstone	Rare solenaporacean red algae, foraminiferal tests and echinoids, common calcispheres and bivalves. Occasional brachiopod shells(?)	5–20	< 1	Moderate
MF 4: Graded grain- to packstone	Occasional brachiopods(?), solenaporacean red algae, crinoid and echinoid fragments, often presenting a micritic coat	0–10	2	Rare
MF 5: Mudstone/wackestone	Rare calcified radiolarians, roveacrinids, ostracods, inoceramids, bivalves, brachiopods, fish remains, and echinoids. Abundant planktonic foraminiferal tests and calcispheres	0–15	4	Moderate to abundant
MF 6: Argilaceous mudstone/wackestone	Abundant planktonic foraminiferal tests. Common calcispheres, calcified radiolarians. Rare roveacrinids, ostracods, echinoids, and fish remains	20–35	4	Abundant
MF 7: Mudrock with allochems	Calcispheres, planktonic and benthonic foraminifera, gastropods, brachiopods, solenaporacean red algae, bivalves, and echinoderms	45–55	5–15	Moderate to abundant
MF 8: Marl	Abundant calcispheres, planktonic foraminiferal tests. Rare calcified radiolarians, benthonic foraminiferal tests, ostracods, bivalves, and fish remains	35–60	0–8	Abundant
MF 9: Mudrock	Abundant planktonic foraminiferal tests. Frequent ammonoids and plant remains. Occasional calcispheres. Rare benthonic foraminiferal tests, calcified radiolarian, brachiopods(?) bivalve shells, echinoid spines, ostracods, fish remains	60–90	5–32	Abundant
MF 10: Fossiliferous mudrock	Abundant foraminiferal tests. Frequent ammonoids and plant remains. Rare calcified radiolarians, ostracods, benthonic foraminiferal tests, bivalves, and fish remains	55–80	0–5	Abundant

bioturbation is very rare, with *Thalassinoides* (Glossifungites ichnofacies) observed in one bed at the top of the well.

Marls are represented by microfacies MF 8 (marl). It is formed by a mixture of clay and micrite in similar proportions, showing a massive or laminated structure. When parallel lamination is observed, it is marked by millimeter-thick alternations of laminae with a predominance of micrite and laminae with a predominance of clay (Fig. 5b). Bioturbation is frequently observed (Fig. 5c).

Mudrocks are abundant in the lowermost part of the well; hence, three microfacies were characterized, mostly composed of terrigenous mud. The microfacies MF 7 (mudrock with allochems) is composed of massive terrigenous mud with different types of poorly sorted allochem grains (silt to gravel in size) dispersed in terrigenous mud (Fig. 5a). Localized convolute and disrupted lamination occur in this microfacies (Fig. 3d). The microfacies MF 9 (mudrock) is composed mainly of terrigenous mud (Figs. 5d, e) with up to 16% bioclasts. Plant remains are frequent (Fig. 3e), micrite is rarely observed and bioturbation is common. The microfacies MF 10 (fossiliferous mudrock) is distinguished by the abundant amount of

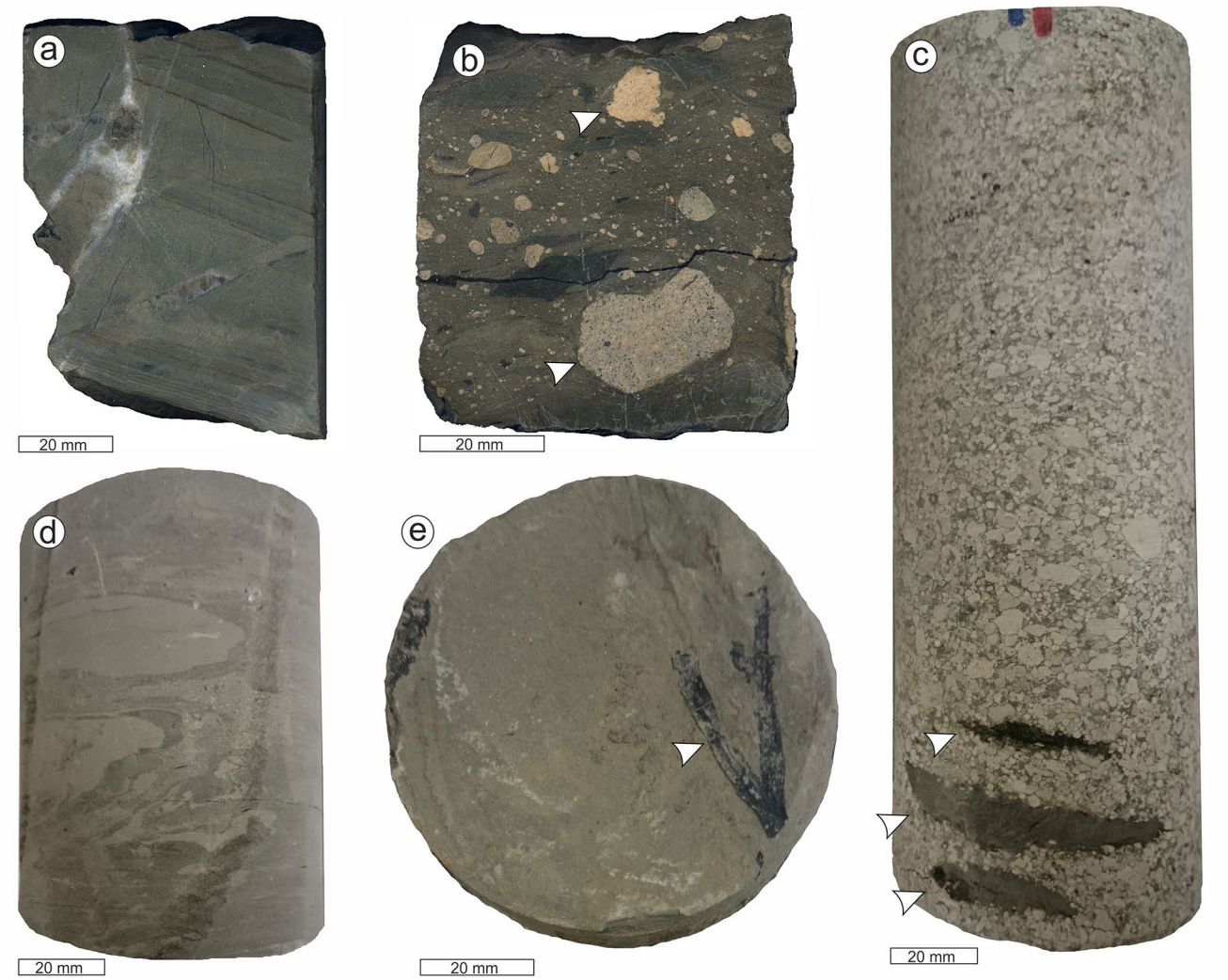

Fig. 3 **a** MF 1: Crystalline dolomite with faults displacing and tilting the original parallel lamination (interval 226.45 m). **b** MF 3: Intraclastic floatstone with wackestones, packstone, and grainstone intraclasts indicated by the arrows (interval 346.60 m). **c** MF 4: Graded grain- to packstone with poor normal grading and mudrock intraclasts at the base indicated by the white arrows (interval 411.90 m). **d** MF 7: Mudrock with allochems presenting well-marked convolute laminae (interval 407.00 m). **e** MF 9: Mudrock with massive structure and plant remains indicated by the white arrow (interval 370.05 m)

bioclasts, mostly planktonic foraminiferal tests (Fig. 5f). Plant remains are rare and the content of organic matter is high (1–4%). In most cases, this microfacies is laminated but the lamination is not a diagnostic feature, rarely showing a massive structure and bioturbation. It presents a variable amount of microcrystalline calcite, which reaches as high as 20%. Microfacies types with these properties were not described by Berthou and Bengtson (1988) and Walter (2000).

Silica nodules occur through the upper part of the section (above 300 m, Fig. 2), mostly in microfacies types MF 1, MF 3, MF 5, MF 8, MF 9, and MF 10. They exhibit a grayish to black color, centimetric size, and are composed of microcrystalline silica.

Interpretation

Microfacies successions were not established in this study due to the nature of the deposits, which in many cases were formed by random episodic events (e.g., debris flows and turbidity currents generated by earthquakes or storms) or by climatic-related deposition. Hence, it interrupted any logic succession that would support the environmental interpretation. Thus, the microfacies vertical pattern was analyzed individually.

The microfacies MF 1 (crystalline dolomite) is always associated with fractured zones, and the original parallel lamination was tilted due to faulting. The size and nearly uniform shape of the dolomite crystals may indicate that

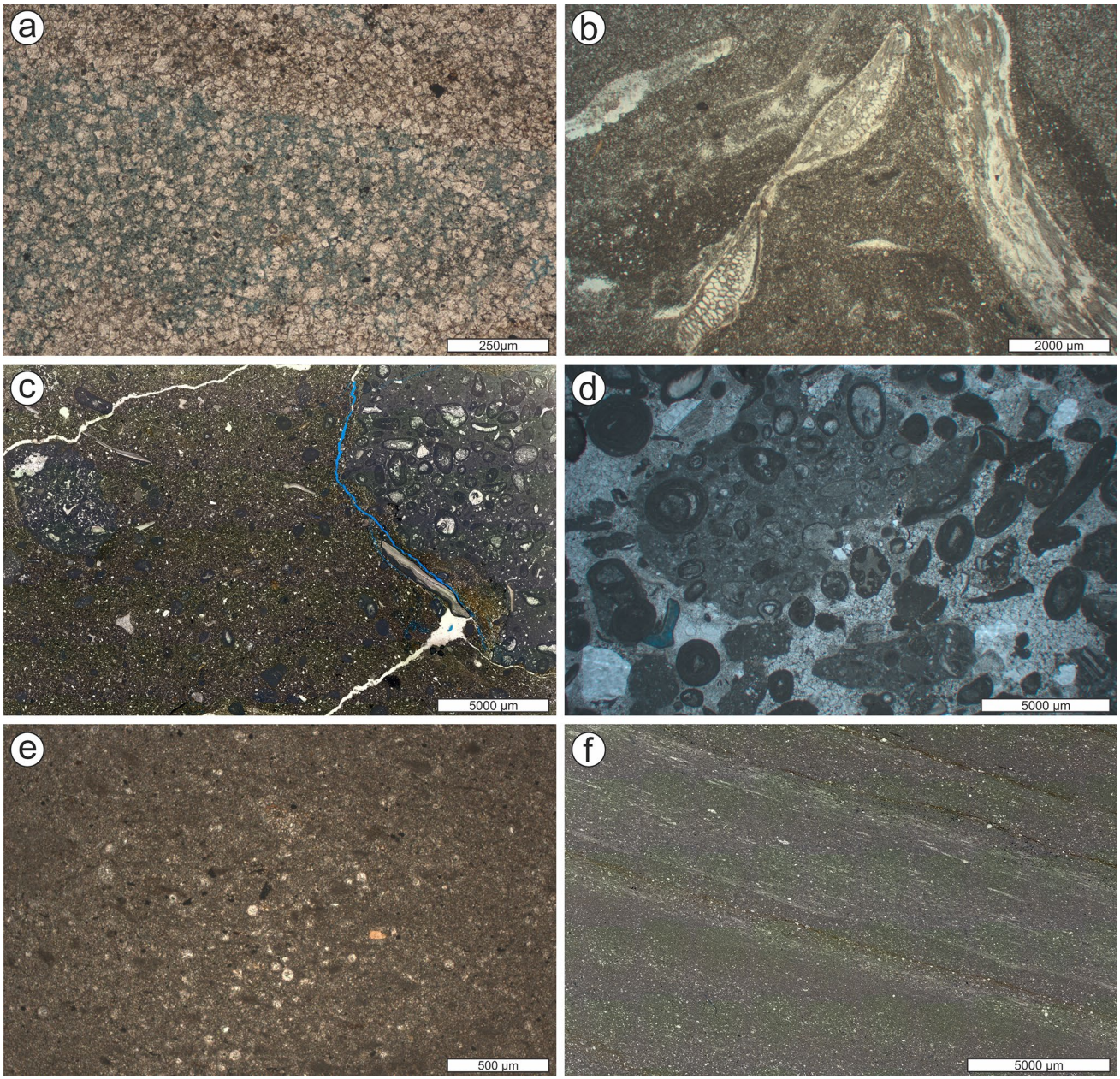

Fig. 4 Photomicrographs of the microfacies types MF 1–5. **a** MF 1: Crystalline dolomite with euhedric to subhedric crystals and intercrystalline porosity in the center (interval 196.30 m, plane polarized light, magnification 10 ×). **b** MF 2: Bioclastic floatstone with coarse bivalve fragments and dolomitized matrix (interval 52.75 m, plane polarized light, magnification 1.25 ×). **c** MF 3: Intraclastic floatstone with packstone intraclasts and bivalve shell fragments (interval 346.60 m, plane polarized light, magnification 2.5 ×). **d** MF 4: Graded grain- to packstone showing ooids, intraclasts, bioclasts, and detrital quartz grains as components (interval 412.70 m, plane polarized light, magnification 2.5 ×). **e** MF 5: Mudstone/wackestone with massive texture, presenting calcispheres, and neomorphized matrix (interval 375.15 m, plane polarized light, magnification 5 ×). **f** MF 5: Mudstone/wackestone with parallel lamination marked by a high concentration of bioclasts or by terrigenous clay. The lamination is tilted due to late tectonic activity (interval 212.5 m, plane polarized light, magnification 5 ×)

the original rock was probably a mudstone or wackestone with small amounts of bioclasts. The dolomitization processes were interpreted as having been formed by percolation of meteoric waters through fractures.

The coarse-grained lithofacies (MF 2, MF 3, MF 4, and MF 7) were interpreted as gravitational flows deposited at the toe of the slope, triggered by short-lived increases in shear stress generated by earthquakes or storms that created

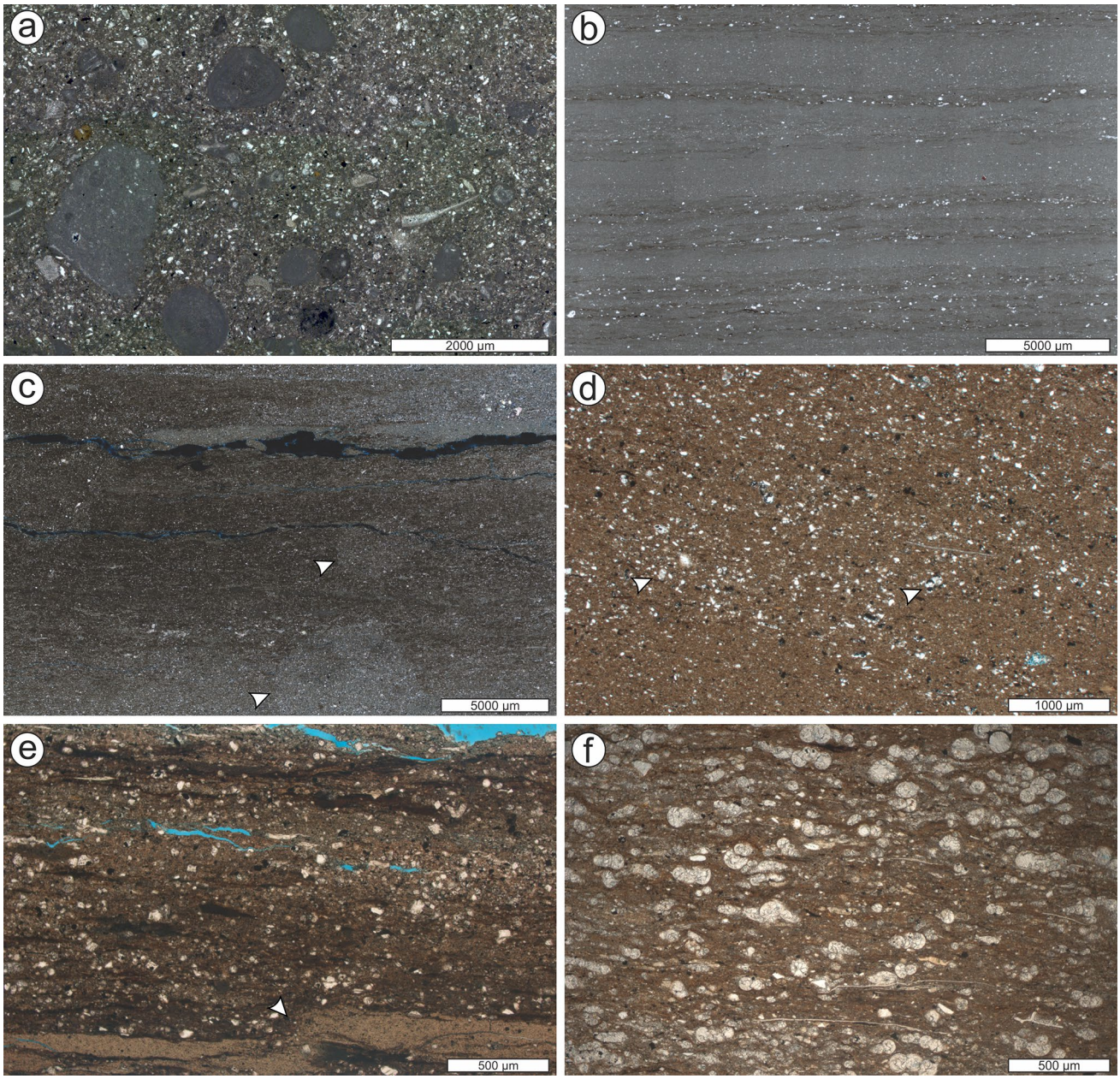

Fig. 5 Photomicrographs of the microfacies types MF 7–10. **a** MF 7: Mudrock with allochems; note bioclasts, peloids, and highly micritized ooids and oncoids (interval 414.00 m, plane polarized light, magnification 2.5 ×). **b** MF 8: Marl characterized by planar-parallel lamination showing an alternation of thicker laminae of micrite and thin laminae of terrigenous clay and organic matter (interval 234.45 m, plane polarized light, magnification 2.5 ×). **c** MF 8: Marl with massive texture showing a mixture of micrite and terrigenous clay. Note the bioturbation indicated by the arrows (interval 408.35, crossed polarized light, magnification 5 ×). **d** MF 9: Mudrock with massive texture presenting elevated amount of quartz and few bioclasts (foraminiferal tests); interval 311.25; plane polarized light; magnification 2.5 ×). **e** MF 9: Mudrock with well-marked lamination disrupted by a small-scale fault (interval 307.35 m, plane polarized light, magnification 5 ×). **f** MF 10: Bioclastic mudrock with abundant planktonic foraminiferal tests immersed in a terrigenous clay matrix (interval 278.1 m, plane polarized light, magnification 5 ×)

the instability necessary for slope collapse (Spence and Tucker 1997). The microfacies MF 2 (bioclastic floatstone) was deposited by a debris flow that transported the shells downslope to a distal subaqueous environment. In terms of texture and the interpreted sedimentary process, this microfacies is similar to the bioclastic floatstone to wackestone facies (F1b) described by El-Asmar et al. (2015) in the Upper Jurassic of Saudi Arabia. The microfacies MF 3 (intraclastic floatstone) was deposited by a cohesive debris flow (Lowe 1982; Mulder and Alexander 2001), as suggested

by the massive texture with intraclasts, poor sorting and the presence of shallow marine grains (e.g., red algae fragments and ooids) associated with planktonic forms (e.g., calcispheres and foraminifera) in a mud matrix. The microfacies MF 4 (graded grain- to packstone) is vertically associated to the microfacies MF 7 (mudrock with allochems). The presence of crude normal grading, erosional contact, and mud intraclasts were attributed to a deposition by a turbulent flow characterized as a poorly efficient flow (Mutti et al. 2003). The microfacies MF 7 (mudrock with allochems) exhibits a bioclastic content represented by a mixture of shallow and deep marine fossils and was formed by a debris flow. The occurrence of localized convolute laminae and disrupted lamination may suggest the debris flow evolved from a slump.

The microfacies MF 5, MF 6, MF 8, MF 9, and MF 10 were interpreted as deposits of carbonate and/or terrigenous mud in a subaqueous low-energy environment. The microfacies MF 5 (mudstone/wackestone) represents carbonate mud deposition in an exaerobic environment (sensu Savrda and Bottjer 1991); the presence of macrofossil remains and bioturbation indicate that this water had enough oxygen to allow the colonization of the substrate. Slight dolomitization occurred in fractured zones. The high clay content of microfacies MF 6 (argillaceous mudstone/wackestone) may have been due to minimal carbonate productivity and/or a high clay input from the continent. *Thalassinoides* ichnogenus is usually associated with firmgrounds, which can indicate a pause in sedimentation (Nieto et al. 2014), interpreted as having been caused by high sea level. The presence of parallel lamination, rare bioturbation, and high pyrite concentrations indicates a quasi-anaerobic environment (sensu Savrda and Bottjer 1991). Similar to microfacies MF 5, it was affected by a slight dolomitization in fractured zones. The microfacies MF 8 (marl) represents the deposition of carbonate mud in alternation with terrigenous mud in a subaqueous low-energy environment. The intercalation was interpreted as a result of cyclic climatic changes. During more humid periods, the terrigenous input from the continent was higher, leading to an increase in the clay content; in drier periods, the terrigenous input was lower and the carbonate production was higher, resulting in the decrease of clay content. Bioturbation was often observed when massive structure was exhibited, suggesting that the lack of lamination was a consequence of burrowing.

Both mudrock microfacies exhibit micritic content, which was interpreted as originating by the smashing of very fine sand-sized peloids. The microfacies MF 9 (mudrock) was interpreted as terrigenous mud deposited in a marine environment close to the continent—suggested by the presence of plant remains together with marine biota (e.g., radiolarian and foraminifera)—enabling the substantial deposition of terrigenous mud sourced by rivers. The microfacies MF 10 (fossiliferous mudrock) was formed by the deposition of terrigenous mud and abundant planktonic bioclasts. The presence of sedimentary lamination associated with high amounts of early diagenetic pyrite indicated an environment with quasi-anaerobic waters (sensu Savrda and Bottjer 1991). The substantial amount of planktonic foraminiferal tests and calcispheres were associated with periods of low sedimentation rates, possibly due to periods of high relative sea level, favoring the concentration of these microfossils.

The radiolarians found in this section showed its original siliceous tests replaced by calcite or pyrite. This process increased the silicate ions in the fluids and induced the diagenetic precipitation of microcrystalline silica as nodules.

The Berthou and Bengtson (1988) microfacies study suggests an open-marine environment for the Cenomanian–Coniacian interval. The authors noted that oxidizing conditions generally found in shallow waters occurred in some areas in addition to deep-water regimes found in most samples and stratigraphic levels. Shallow waters with oxidizing conditions were not observed herein due to the geographic location of this study (structural low). The deep-water environment with periodic anoxic conditions observed here, however, confirms the previous knowledge of these authors. In addition, Berthou and Bengtson (1988) did not observe the mudrock microfacies described in this study. Indeed, most microfacies with high terrigenous clay content were associated herein to the late Albian (Riachuelo Formation), which was not studied by them.

Organic geochemistry

Total organic carbon (TOC) vs. sulfur (S) plots have proved to be useful to support paleoenvironmental interpretations; Leventhal (1982, 1995) used TOC vs. S plots to define euxinic environments when comparing the results obtained from the Black Sea. The author proposed that high TOC and S values suggest anoxic bottom water conditions capable of preserving organic matter, while low values may indicate oxic conditions.

In the studied section, most of the sample data points were located between the normal marine and the euxinic fields in the Leventhal (1995) plot (Fig. 6). Samples from deeper intervals in the well were plotted nearer the euxinic field, while samples obtained from shallower depths were plotted nearer the normal marine field, indicating a trend of oxygen availability that increased from the base to the top of the well. The hatched area indicates a diagenetic sulfidation overprint due to changes in environmental conditions, also suggesting that part of the base of the well was affected by diagenetic sulfidation, corroborated by the elevated pyrite concentration observed in samples and thin-sections.

The pseudo-Van Krevelen diagram (Fig. 7) of Rock–Eval data indicates a type II kerogen for every sample location

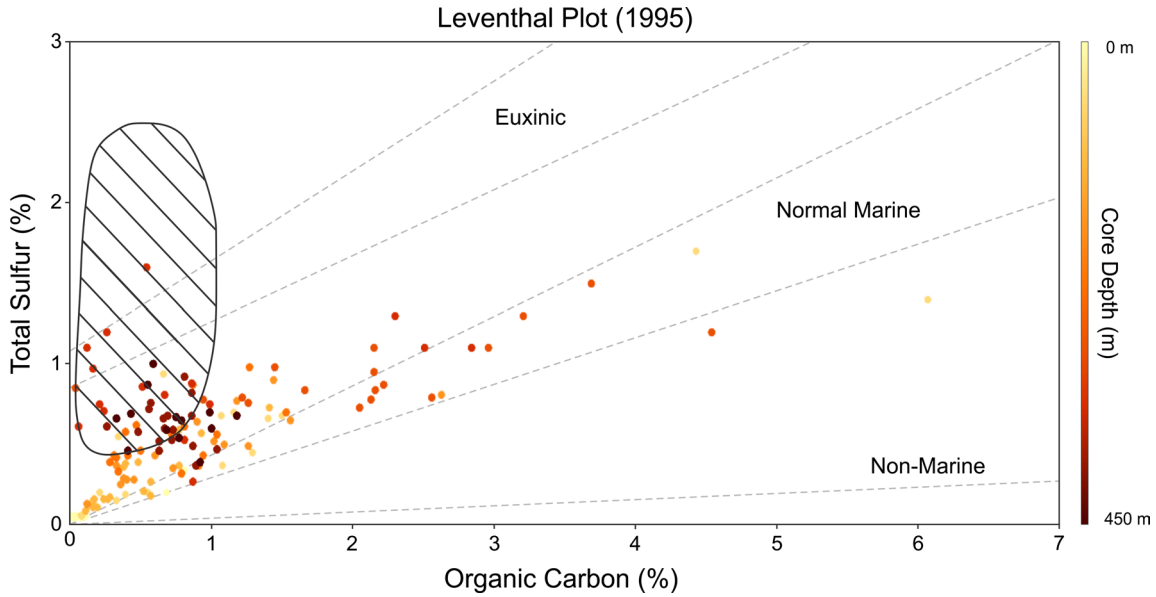

Fig. 6 Results of geochemical analyses plotted in Leventhal's (1995) cross plot colored according to their depths in the well. The *hatched area* corresponds to samples that were affected by diagenetic sulfidation

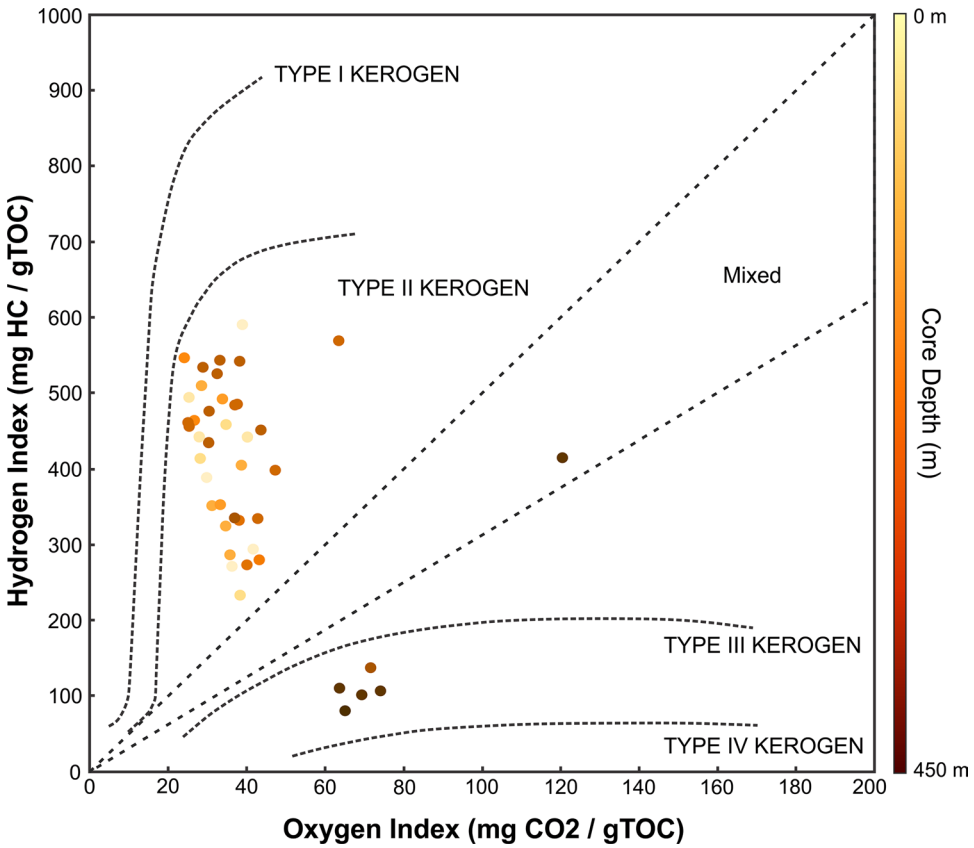

Fig. 7 Pseudo-Van Krevelen diagram of hydrogen and oxygen indices used for chemical classification of organic matter

shallower than 317 m, which was derived mainly from algal organic matter (phytoplankton and zooplankton) but also from pollens and spores and was interpreted as being deposited in marine environments. The deeper sampled interval presented predominantly a type III kerogen, with one sample showing a mixed kerogen (types II and III), which suggests an additional contribution of terrestrial organic matter. The presence of continent-derived organic matter at the bottom

part of the core and of marine-derived organic matter at the upper part of the core indicates a reduction of the continent contribution, possibly due an increase of the relative sea level.

Sequence stratigraphy

Three third-order depositional sequences (sequence 1, sequence 2, and sequence 3) were identified (Fig. 8), bounded by maximum flooding surfaces (mfs 1–mfs 3). Internally, lower-order sequences were recognized; however, they have not been detailed in this study because these sequences did not encompass the scale used here and are, indeed, less relevant to the proposed stratigraphic model. The designation of the sequences followed its upper limits (sequence boundaries). In summary, the studied section represented a transgressive event that began in the early Cenomanian.

The characterization of depositional sequences is based on the integrated data analyses (microfacies, fossil content, gamma ray, TOC, and type of kerogen). The genetic stratigraphy sequences of Galloway (1989) were used because surfaces of maximum flooding are well developed and represented across most of the marine sections (shallow to deep settings), being easier to identify than subaerial exposure surfaces that are mostly well developed in shallower settings and might be missing in deeper settings.

The stratigraphic age framework was established based on: (1) last occurrence of the species *Braarudosphaera africana*, top of the biozone N-252 (Albian/Cenomanian boundary) of Antunes (1997); (2) first occurrence of the species *Eprolithus octopetalus*, top of Subzone UC5c (Cenomanian/Turonian boundary) of Burnett (1998); and (3) occurrence of the species *Radiolithus planus*, which is placed by Young et al. (2017) in the lower Turonian. The calcareous nannofossils were absent in the uppermost part of the section.

Sequence 1 consisted of microfacies MF 3, MF 4, MF 5, MF 7, MF 8, MF 9, and MF 10. In the beginning, it represents a deposition of gravity flows near the slope of a mixed carbonate-siliciclastic platform during a sea-level lowstand. It was evidenced by the presence of reworked microfacies (MF 3, MF 4, and MF 7) with coated grains and red algae debris, and the presence of low-energy microfacies (MF 5, MF 8, MF 9, and MF 10); some of the microfacies are bioturbated and/or exhibiting plant remains. Later, a relative sea-level rise caused a transgression, marked by an increase in planktonic foraminifera content (MF 10) and in organic matter content. The rise in the base level led to a considerable reduction of the amount of delivered terrigenous sediment. The predominance of laminated facies, the peak in the TOC, and the predominance of the planktonic fossil content marked the maximum flooding surface and the sequence limit.

Sequence 2 consisted of microfacies MF 1, MF 5, MF 6, MF 8, MF 9, and MF 10. This sequence starts with a progradation of carbonate deposits during a sea-level highstand, represented by the reduction of the terrigenous clay content, with deposition of carbonate mud (MF 5, MF 6, and MF 8), indicating an increase in the carbonate factory contribution. In this sequence, characteristic features of a sea-level drop could not be observed. Three possibilities, not mutually exclusive, were assumed: (1) correlative conformities "hiding" the presence of such features; (2) the presence of normal faults omitting the sea-level drop interval; and (3) a rise in the relative sea level immediately following a sea-level highstand without a sea-level drop. The transgression was marked by the presence of highly laminated mudstones and wackestones and by an increase in the planktonic fauna and the increase in organic matter content. A peak in the TOC and a peak in the planktonic fossil content were interpreted as the maximum flooding surface, which was accompanied by an increase in argilosity (MF 6) and marked the superior limit of this sequence.

Sequence 3 consisted of microfacies MF 1, MF 2, MF 3, MF 5, MF 6, and MF 8. Its beginning is marked by the progradation of the carbonate ramp and the increase of the carbonate mud content (MF 5) in relation to terrigenous mud. Part of this interval was highly affected by tectonic activity and shows a high frequency of fracture networks, faults, and pervasive dolomitization, which made it difficult to form an accurate stratigraphic interpretation (Fig. 9). The presence of highly burrowed mudstones and wackestones indicated a relative sea-level drop, which was also evidenced by the presence of intraformational floatstones (MF 3) with wackestone and mudstone intraclasts, representing olitostromes formed by cohesive debris flows and slumps at the toe of slope. The rise in argilosity (MF 6 and MF 8), increase in organic content, and the presence of laminated microfacies (MF 5, MF 6, and MF 8) marked a rise in relative sea level, which achieved its maximum flooding (MFS) at the 61-m section interval, as evidenced by a TOC peak and the presence of *Thalassinoides* ichnogenus. The upper limit of this sequence was placed at the base of the dolomitized, karstified, and weathered section.

Campos Neto et al. (2008) recognized two depositional sequences (K70–K84 and K86–88) in the studied interval bounded by regressive surfaces and with a different stratigraphic order of that used herein. In this study, sequence boundaries were delimited by maximum flooding surfaces (Galloway 1989). Hence, the dating of the sequence boundaries observed here were different from those of Campos Neto et al. (2008), making a comparison between them impossible.

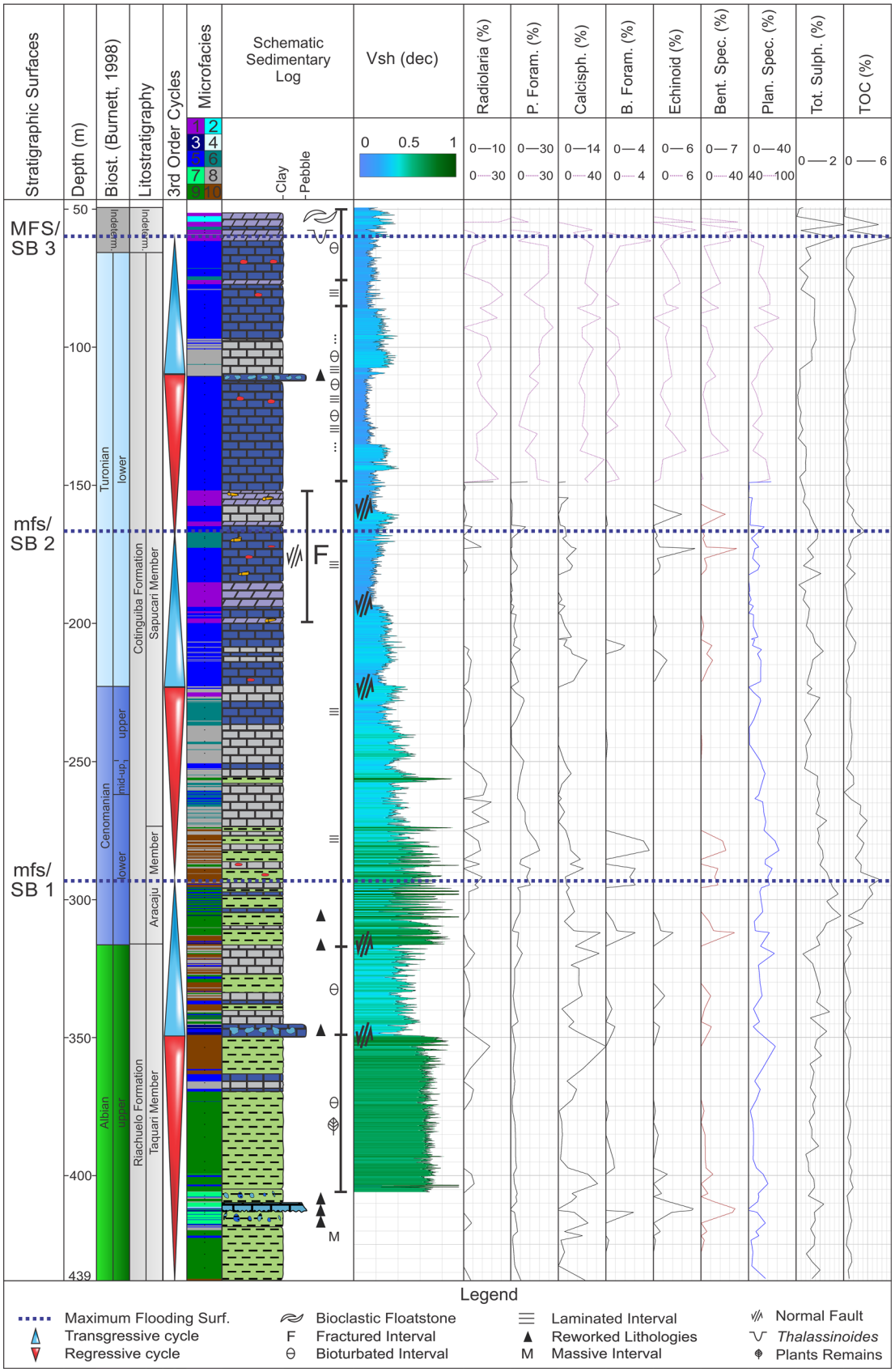

Fig. 8 Integrated analysis of the studied section presenting the three recognized cycles and the stratigraphic surfaces. The *gray biostratigraphic zone* in the upper part represents areas with no nannofossils recuperation due to limited preservation of samples

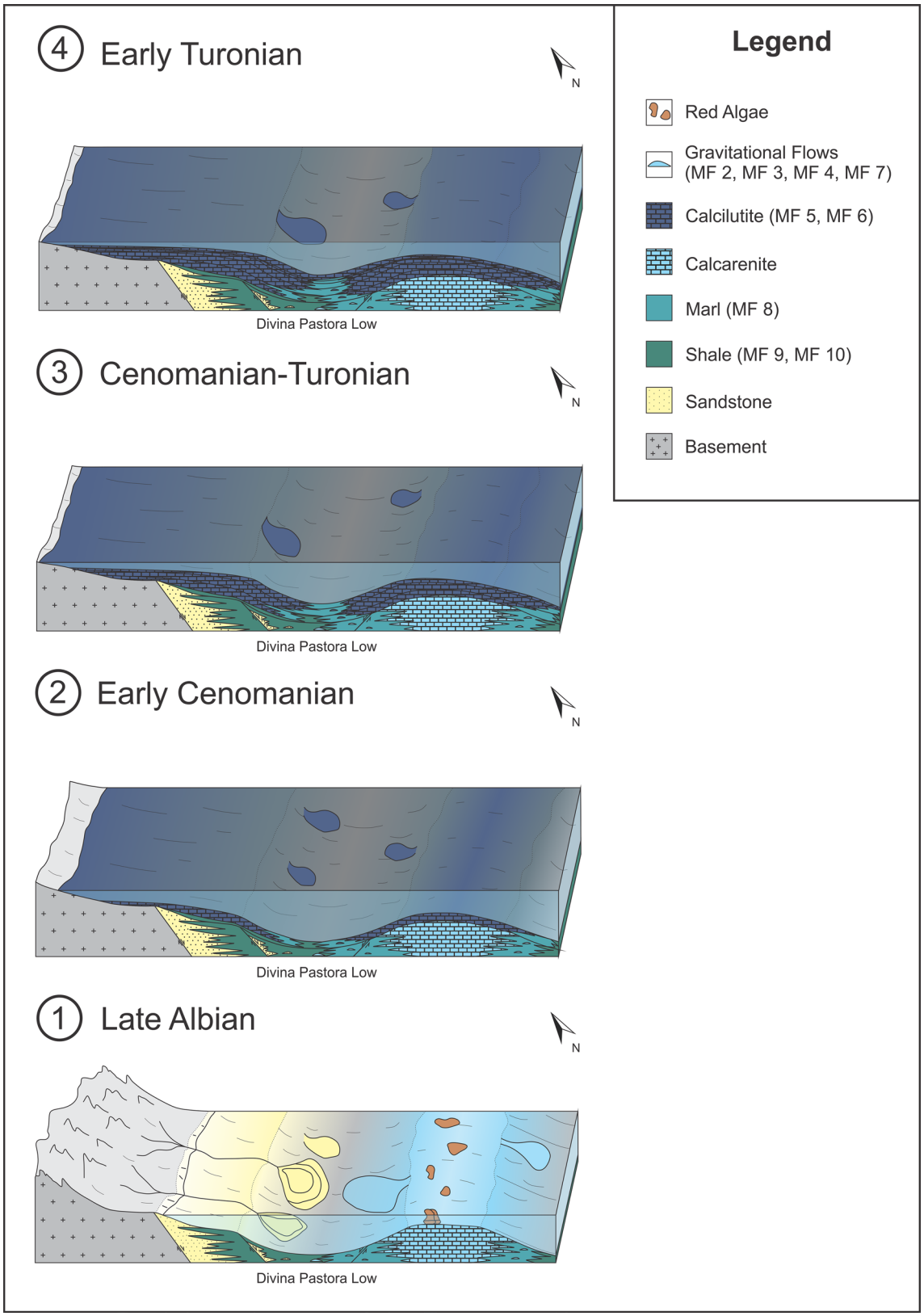

Fig. 9 Paleoenvironmental evolution of the Divina Pastora structural low from the late Albian to the early Turonian. **a** Late Albian partially protected carbonate-siliciclastic mixed platform. **b** Early Cenomanian distally steepened carbonate ramp. **c** Cenomanian–Turonian progradation of carbonate ramp. **d** Early Turonian marking the higher influence of the carbonate factory due to low terrigenous influx

Paleoenvironmental evolution

The detailed study of the defined sequences, supported by the available literature (e.g., Koutsoukos 1989; Koutsoukos et al. 1991, 1993), allowed for the interpretation of the depositional system and its evolution at the Divina Pastora Low. The depositional environment evolved from a partially protected carbonate-siliciclastic mixed platform (lithostratigraphically correlatable to the Riachuelo Formation) to a distally steepened carbonate ramp (lithostratigraphically associated with the Cotinguiba Formation).

The studied core was divided into four intervals with distinct sedimentological and stratigraphic characteristics: late Albian, early Cenomanian, Cenomanian–Turonian, and early Turonian.

The late Albian interval was associated with a partially protected carbonate-siliciclastic mixed platform (Fig. 9a), with deeper portions in structural lows (e.g., the Divina Pastora Low, see Fig. 1). The presence of terrigenous material, plant remains (MF 8), and the mixture between kerogen of types II and III suggested a constant influx from the continent associated with a more humid climatic phase and possibly renewed source areas uplifted by tectonic activity (Campos Neto et al. 2008). The occurrence of allochem grains (sometimes supported by terrigenous muddy matrix) at deeper parts (the Divina Pastora Low) was interpreted as the occurrence of gravitational flows (MF 3, MF 4, MF7) triggered by earthquakes or storms that originated at oolitic/oncolitic shoals formed at adjacent structural highs (e.g., Aracaju High, see Fig. 1).

The early Cenomanian interval was associated with a rise in sea level, responsible for the drowning of the oolitic shoals and continental source areas. The rise of the base level led to the reduction in the amount of terrigenous material and continent-derived organic matter transported by rivers due to a smaller fluvial gradient. This period was tectonically stable with denuded source areas and lower terrigenous input. Therefore, the scarcity of terrigenous material favored the carbonate productivity and provided the necessary conditions to form a distally steepened carbonate ramp (Fig. 9b) morphologically associated with the Divina Pastora Low. The sediment deposition was heavily influenced by variations in carbonate production and climatic changes. As a result, calcilutites (MF 5 and MF 6) occurred interbedded with marls (MF 8) and shales (MF 9 and MF 10). In addition, the presence of carbonate breccias (MF 3) indicated the occurrence of gravitational flows triggered by short-lived events that increased the shear stress in the slope, such as earthquakes or storms.

The Cenomanian–Turonian interval (Fig. 9c) represents the progradation of the carbonate ramp driven by an increase in the deposition of carbonate mud and the continuous decrease in argilosity (MF 5, MF 6, and MF 8). In the beginning, the sea level remained constantly high and a further transgression occurred without a marked sea-level drop, as discussed in the sequential analysis (see section Sequence Stratigraphy). Episodes of oxygen deficiency developed, intensified by the rise in sea level that expanded the minimum oxygen layer, causing the extinction of many species and favoring the deposition of laminated facies. The transgression on the Cenomanian–Turonian interval observed in the studied section agrees with other studies of the Sergipe–Alagoas Basin (e.g., Berthou and Bengtson 1988; Mello et al. 1989; Koutsoukos 1992; Koutsoukos et al. 1993; Seeling and Bengtson 2002). However, Walter et al. (2005), studying an outcrop ca. 20 m thick in the Japaratuba area (approximately 30 km to northeast, Fig. 1), noted a shallowing-upward trend in this same time interval. This sharp contrast can be explained by the differential subsidence related to basement tectonics in this period (Berthou and Bengtson 1988).

The early Turonian interval (Fig. 9d) was marked by a higher influence of the carbonate factory and almost no influence of continental sediments due to tectonic quiescence and the possibility of an arid climate. This interval shows a predominance of mudstones and wackestones (MF 5) and carbonate breccias (MF 3) with mudstones and wackestones intraclasts. The carbonate breccias were interpreted as being caused by earthquakes that destabilized the slope that collapsed and evolved into gravity flows. During this interval, the sea level is considered the maximum of the entire studied section, as evidenced by the highest level of TOC and the occurrence of *Thalassinoides* ichnogenus, indicating the presence of a firmground formed by a low sedimentation rate.

Conclusions

In this study, the analysis of 439 m of continuous core resulted in the establishment of ten sedimentary microfacies types, which were related to a paleoenvironmental interpretation. The late Albian–early Turonian succession in the Sergipe–Alagoas Basin was deposited on a partially protected carbonate-siliciclastic mixed platform with a gradual passage to a carbonate ramp morphologically associated with a structural low.

The integrated approach of sedimentology, geochemistry, microfacies, and gamma ray analyses provided substantial information to support the paleoenvironmental interpretation when studying deep-marine deposits. These analyses were crucial in recognizing microfossil abundance, argilosity, and TOC variations, which contributed to the definition of flooding surfaces to establish depositional sequences and

to understand the paleoenvironmental evolution in the study area.

During the late Albian, the sedimentation is considered to have been highly controlled by tectonic activity and climate. Further, the tectonic activity ceased and the carbonate productivity increased following the Cenomanian, with the climate acting as the primary mechanism controlling the sedimentation.

The stratigraphy reflects a transgression that drowned a shallower platform and the source areas. Three genetic sequences were bounded by maximum flooding surfaces due to a lack of features, indicating subaerial exposures. Hence, the evolution of the Divina Pastora structural low from the late Albian to the early Turonian can be summarized as a transgressive event that drowned source areas and favored the implementation of a carbonate ramp. Indeed, it can be divided into three phases: the first, a partially protected carbonate-siliciclastic mixed platform; the second, a sea-level rise causing the drowning of source areas; and the third, implementation of the carbonate ramp and consolidation of carbonate sedimentation.

Acknowledgements This research was carried out in association with the ongoing R&D project registered as ANP 20225-9, "PRESALT—Geological characterization of carbonate reservoirs from the pre-salt interval of Santos Basin, correlates (Sergipe–Alagoas Basin) and analogues" (UFRJ/Shell Brasil/ANP), sponsored by Shell Brasil. We thank Votorantim Cimentos S.A., Laranjeiras unit, for the drilling authorization at its facilities. We furthermore thank the reviewers Peter Bengtson and Herbert Volk for the critical reading, careful recommendations, and constructive criticism that greatly improved this paper. PFD thanks CNPq (process 310164/2017-6) for the research Grant.

References

Ahr WM (1973) The carbonate ramp: an alternative to the shelf model. Trans Gulf Coast Assoc Geolo Soc 23:221–225

Alves T, Cooper M, Rios-Netto A (2016) Paleogene-Neogene calcareous nannofossil biostratigraphy and paleoecological inferences from northern Campos Basin, Brazil (well Campos-01). J S Am Earth Sci 71:143–160

Andrade EJ (2005) Turonian inoceramids and biostratigraphy of the Sergipe Basin, northeastern Brazil: an integrated study of the Votorantim and Nassau quarries. Dissertation, Ruprecht-Karls-Universität Heidelberg

Antunes RL (1997) Introdução ao estudo de nanofósseis calcários. Instituto de geociências, Rio de Janeiro

Bandeira AN Jr (1978) Sedimentologia e microfacies calcárias das Formações Riachuelo e Cotinguiba da Bacia Sergipe/Alagoas. Boletim Técnico da Petrobrás 21:17–69

Bengtson P (1983) The Cenomanian–Coniacian of the Sergipe Basin, Brazil. Fossils Strata 12:1–78

Berthou P-Y, Bengtson P (1988) Stratigraphic correlation by microfacies of the Cenomanian–Coniacian of the Sergipe Basin, Brazil. Fossils Strata 21:1–88

Burnett JA (1998) Upper Cretaceous. In: Bown PR (ed) Calcareous Nannofossil biostratigraphy. British micropaleontology society publications series. Kluwer Academic Publishers, London, pp 132–199

Campos Neto OPA, Souza Lima W, Gomes Cruz FE (2008) Bacia de Sergipe–Alagoas. Boletim de Geociências da Petrobras 15 [for 2007]:405–415

Carozzi AV (1989) Carbonate rocks depositional model. Prentice Hall, Upper Saddle River

El-Asmar HM, Assal EM, El-Sorogy AS, Youssef M (2015) Facies analysis and depositional environments of the Upper Jurassic Jubaila Formation, Central Saudi Arabia. J Afr Earth Sc 110:34–51

Embry AF, Klovan JE (1972) Late Devonian reef tracts on northeastern Banks Islands, Northwest Territories. Can Pet Geol Bull 19:730–781

Flügel E (2004) Microfacies of carbonate rocks, analysis, interpretation and application. Springer, Berlin

Friedman GM (1959) Identification of carbonate minerals by staining methods. J Sediment Petrol 29:87–97

Galloway WE (1989) Genetic stratigraphic sequences in basin analysis I: Architecture and genesis of flooding-surface bounded depositional units. Am Assoc Pet Geol Bull 73:125–142

Grabau AW (1904) On the classification of sedimentary rocks. Am Geol 33:228–247

Haq BU (2014) Cretaceous eustasy revisited. Global Planet Change 113:44–58

Hessel MHR (1988) Lower Turonian inoceramids from Sergipe, Brazil: systematics, stratigraphy and palaeoecology. Fossils Strata 22:1–49

Koutsoukos EAM (1989) Mid- to late Cretaceous microbiostratigraphy, paleo-ecology and paleogeography of the Sergipe–Basin, northeastern Brazil. Dissertation, Polytechnic South West

Koutsoukos EAM (1992) Late Aptian to Maastrichtian foraminiferal biogeography and palaeoceanography of the Sergipe Basin, Brazil. Palaeogeogr Palaeoclimatol Palaeoecol 92:295–324

Koutsoukos EAM, Mello MR, Azambuja Filho NC (1991) Micropaleontological and geochemical evidence of mid-Cretaceous dysoxic–anoxic paleoenvironments in the Sergipe Basin, northeastern Brazil. In: Tyson RV, Pearson TH (eds) Modern and ancient continental Shelf Anoxia. Geological Society Special Publication 58:427–447

Koutsoukos EAM, Destro N, Azambuja Filho NC, Spadani AR (1993) Upper Aptian-lower Coniacian carbonate sequences in the Sergipe Basin, northeastern Brazil. In: Simo T, Scott RW, Masse J-P (eds) Cretaceous carbonate platforms. AAPG Memoir, pp 127–144

Lana MC (1990) Bacia de Sergipe–Alagoas: uma hipótese de evolução tectono-sedimentar. In: Raja Gabaglia GP, Milani EJ (eds) Origem e Evolução de Bacias Sedimentares. Editora Gávea, Rio de Janeiro, pp 311–332

Leventhal JS (1982) An interpretation of carbon and sulfur relationships in Black Sea sediments as indicators of environments of deposition. Geochim Cosmochim Acta 47:133–137

Leventhal JS (1995) Carbon-sulfur plots to show diagenetic and epigenetic sulfidation in sediments. Geochim Cosmochim Acta 59:1207–1211

Mello M, Koutsoukos E, Hart M, Brassell S, Maxwell JR (1989) Late Cretaceous anoxic events in the Brazilian continental margin. Org Geochem 14:529–542

Mutti E, Tinterri R, Benevelli G, di Biase D, Cavanna G (2003) Deltaic, mixed and turbidite sedimentation of ancient foreland basins. Mar Pet Geol 20:733–755

Nieto LM, Rodríguez-Tovar FJ, Molina JS, Reolid M, Ruiz-Ortiz PA (2014) Unconformity surfaces in pelagic carbonate environments: a case from the middle Bathonian of the Betic Cordillera, SE Spain. Ann Soc Geol Pol 84:281–295

Ojeda HAO, Fugita AM (1976) Bacia Sergipe/Alagoas: geologia regional e perspectivas petrolíferas. In: Congresso Brasileiro de Geologia. Porto Alegre, SBG, vol 28, pp 137–158

Poupon A, Gaymard R (1970) The evaluation of clay content from logs. SPWLA 11th Annual Logging Symposium, Conference paper: 1970-G

Read JF (1982) Carbonate platforms of passive (extensional) continent margins: types, characteristics and evolution. Tectonophysics 81:195–212

Savrda CE, Bottjer DJ (1991) Oxygen-related biofacies in marine strata: an overview and update. In: Tyson RV, Pearson TH (eds) Modern and Ancient Continental Shelf Anoxia. Geological Society Special Publication, pp 201–219

Schaller H (1970) Revisão estratigráfica da Bacia de Sergipe/Alagoas. Boletim Técnico da Petrobras 12 [for 1969]:21–86

Schlanger SO, Jenkyns HC (1976) Cretaceous oceanic anoxic events: causes and consequences. Geol Mijnbouw 55:179–184

Seeling J, Bengtson P (2002) Palaeobiogeography of the upper Cenomanian-lower Turonian macroinvertebrates of the Sergipe Basin, northeastern Brazil. In: Wagreich M (eds) Aspects of the Cretaceous Stratigraphy and Palaeobiogeography. Schriftenreihe der Erdwissenschaftlichen Kommissionen der Österreichen Akademie der Wissenschaften, vol 15, pp 151–168

Spence GH, Tucker ME (1997) Genesis of limestone megabreccias and their significance in carbonate sequence stratigraphic models: a review. Sed Geol 112:163–193

Tucker ME (1985) Shallow-marine carbonate facies and facies models. In: Brenchley P, Williams BPJ (eds) Sedimentology, recent developments and applied aspects. Geological Society Special Publication, London, pp 147–169

Walter S (2000) Palaeoenvironmental analysis of the upper Cenomanian and lower Turonian limestone beds in the Sergipe Basin, northeastern Brazil, based on microfacies analysis, micropalaeontology, and stable isotopes, Ruprecht-Karls-Universität Heidelberg

Walter S, Herrmann AD, Bengtson P (2005) Stratigraphy and facies analysis of the Cenomanian–Turonian boundary succession in the Japaratuba area, Sergipe Basin, Brazil. In: Bengtson P (eds) Mesozoic palaeontology and stratigraphy of South America and the South Atlantic, Part II. J South Am Earth Sci 19:273–283

Wilson JL (1975) Carbonate facies in geologic history. Springer, New York

Young JR, Bown PR, Less JA (2017) Nannotax3 website. International nannoplankton association. http://www.mikrotax.org/Nannotax3/. Accessed 21 April 2017